arXiv:1503.01517v2 [gr-qc] 1 Oct 2015

Maximum mass of a barotropic spherical star

Atsuhito Fujisawa

Department of Physics, Nagoya University, Chikusa-ku, 464-8602 Nagoya, Japan

E-mail: `fujisawa@gravity.phys.nagoya-u.ac.jp`

Hiromi Saida

Department of Physics, Daido University, Minami-ku, 457-8530 Nagoya, Japan

E-mail: `saida@daido-it.ac.jp`

Chul-Moon Yoo and Yasusada Nambu

Department of Physics, Nagoya University, Chikusa-ku, 464-8602 Nagoya, Japan

E-mail: `yoo@gravity.phys.nagoya-u.ac.jp`

E-mail: `nambu@gravity.phys.nagoya-u.ac.jp`

Abstract. The ratio of total mass m_* to surface radius r_* of spherical perfect fluid ball has an upper bound, $Gm_*/(c^2 r_*) \leq \mathcal{B}$. Buchdahl obtained $\mathcal{B}_{\rm Buch} = 4/9$ under the assumptions; non-increasing mass density in outward direction, and barotropic equation of state. Barraco and Hamity decreased the Buchdahl's bound to a lower value $\mathcal{B}_{\rm BaHa} = 3/8$ $(< 4/9)$ by adding the dominant energy condition to Buchdahl's assumptions. In this paper, we further decrease the Barraco-Hamity's bound to $\mathcal{B}_{\rm new} \simeq 0.3636403$ $(< 3/8)$ by adding the subluminal (slower-than-light) condition of sound speed. In our analysis, we solve numerically Tolman-Oppenheimer-Volkoff equations, and the mass-to-radius ratio is maximized by variation of mass, radius and pressure inside the fluid ball as functions of mass density.

PACS numbers: 04.40.-b , 95.30.Sf

Submitted to: *Class. Quantum Grav. (accepted for publication)*

1. Introduction and summary of result

A question of self-gravitating compact object is the subject of this paper: How much weight or how small radius can a compact object possess? A quantitative answer is given by the mass-to-radius ratio $Gm_*/(c^2 r_*)$, where m_* and r_* are respectively the total mass and surface radius of compact object. Assuming static spherical symmetry for simplicity, which implies the outside region of compact object is Schwarzschild geometry, this ratio is bounded above, $Gm_*/(c^2 r_*) \le \mathcal{B}$. The upper bound needs to satisfy, $\mathcal{B} < 1/2$ ($\Leftrightarrow 2Gm_*/c^2 < r_*$), in order to avoid gravitational collapse.

An interesting issue of this bound is whether $\mathcal{B}$ is less than 1/3 or not. If an inequality, $\mathcal{B} \ge 1/3$ ($\Leftrightarrow 3Gm_*/c^2 \ge r_*$), holds for static spherical case, unstable circular orbits of photons can appear in the outside Schwarzschild geometry. If such super-compact object, which possesses unstable circular orbits of photons but no black hole horizon, do neither emit nor reflect any radiation, then we cannot distinguish it from black holes by observing the so-called black hole shadows. Here, the black hole shadow is a dark region which is expected to appear in a fine image of optical/radio observation of black holes (see [1, 2] and references therein): Consider a case that an optical source is extended behind a black hole and does not enter the inside of unstable circular orbits of photons. Observer cannot detect photons which passed through unstable circular orbits inward, because those photons are absorbed by black hole eventually. Hence, in the image of optical source, there should appear the dark region, on which those photons would be detected if black hole did not exist. This dark region is the black hole shadow, and the boundary of shadow is determined by the photons propagating on null geodesics winding many times around unstable circular orbits of photons. This means that a super-compact object possessing unstable circular orbits but no black hole horizon can provide us the same optical image of shadow with black holes. Since the resolution of image by radio observation is now approaching the visible angular size of largest black hole candidate [3, 4], an investigation of possible super-compact object seems to be an important issue for near future observational study of black holes. Therefore, an interesting and important issue is whether $\mathcal{B} < 1/3$ holds or not.

Some exotic models of super-compact objects have been proposed such as gravastars, boson stars and so on. The gravastar as super-compact object has already been examined [5], whereas the others remain to be examined. Those exotic models may be interesting. However, in this paper, we focus on a rather usual model.

Assuming that (i) the compact object is a static spherical ball of perfect fluid, (ii) its mass density is non-increasing with respect to radial coordinate, and (iii) its equation of state is barotropic, Buchdahl obtained $Gm_*/(c^2 r_*) \le \mathcal{B}_{\rm Buch} = 4/9$ [6, 7]. Furthermore, by adding the dominant energy condition to Buchdahl's assumptions, Barraco and Hamity decreased the Buchdahl's bound to a lower value $\mathcal{B}_{\rm BaHa} = 3/8\,(< 4/9)$ [8]. However, this upper bound is greater than $1/3$ $(< \mathcal{B}_{\rm BaHa})$.

Other works on the bound $\mathcal{B}$ have been performed. For example, an effect of cosmological constant is examined [9], a case with infinite surface radius is analyzed [10], and a tangential pressure is considered [11]. However, the Barraco-Hamity's bound, $\mathcal{B}_{\mathrm{BaHa}} = 3/8$, has not been lowered so far.

As explained in detail in section 2, we add the subluminal (slower-than-light) condition of sound speed to the assumptions of Buchdahl and Barraco-Hamity. We discuss, in section 2, how the subluminal-sound-speed condition restricts the form of equation of state, and also that this condition is more restrictive than the dominant energy condition. Then, our upper bound is lower than the Barraco-Hamity's bound,

$$\frac{Gm_*}{c^2 r_*} \le \mathcal{B}_{\mathrm{new}} \simeq 0.3636403 \quad \left(< \mathcal{B}_{\mathrm{BaHa}} = \frac{3}{8} \right) . \tag{1}$$

The reason why $\mathcal{B}_{\mathrm{new}}$ is approximate value is that we have performed numerical integration of Tolman-Oppenheimer-Volkoff equations. Although the upper bound is lowered, it still remains greater than $1/3$ ($< \mathcal{B}_{\mathrm{new}}$). Therefore, at present, we cannot deny the possibility that the same shadow image can be obtained from black holes and some super-compact object made of fluid matter. In order to sharpen the upper bound of $Gm_*/(c^2 r_*)$, some other condition should be assigned to the form of equation of state. (We will report the case of polytropic equation of state in the other paper.)

Section 2 is devoted to the details of our analysis. Section 3 is for conclusion and discussions.

2. Variational analysis of mass-to-radius ratio

2.1. Definitions and assumptions

As explained in section 1, we are interested in a static and spherically symmetric perfect fluid ball. A line element of spacetime is

$$\mathrm{d}s^2 = g_{\mu\nu} \mathrm{d}x^\mu \, \mathrm{d}x^\nu = -e^{2\Phi(r)} c^2 \mathrm{d}t^2 + \frac{\mathrm{d}r^2}{1 - 2Gm(r)/(c^2 r)} + r^2 (\mathrm{d}\theta^2 + \sin^2\theta \mathrm{d}\varphi^2) \, , \tag{2}$$

where (t, r, θ, φ) is spherical poler coordinates, $\Phi(r)$ gives a lapse function, and $m(r)$ is a mass of perfect fluid contained in spherical region of radius r. The stress-energy-momentum tensor of perfect fluid is $T_{\mu\nu} = \sigma(r) c^2 u_\mu u_\nu + p(r) \, (g_{\mu\nu} + u_\mu u_\nu)$, where $u = e^{-\Phi} \partial_{ct}$ is a four-velocity of static perfect fluid, and $\sigma(r)$ and $p(r)$ are respectively a mass density and pressure of perfect fluid.

By the regularity of spacetime at centre, a condition $m(0) = 0$ holds. This implies that the mass density at centre $\sigma_{\mathrm{c}} = \sigma(0)$ is finite. We normalize all quantities by σ_{c},

$$R := \frac{\sqrt{G\sigma_{\mathrm{c}}}}{c} r \quad , \quad \Sigma(R) := \frac{\sigma(r)}{\sigma_{\mathrm{c}}} \quad , \quad M(R) := \frac{\sqrt{G^3 \sigma_{\mathrm{c}}}}{c^3} m(r) \quad , \quad P(R) := \frac{p(r)}{\sigma_{\mathrm{c}} c^2} \, . \tag{3}$$

These are dimension-less. The lapse function, $\Phi(r) := \Phi(R)$, does not need normalization because Φ is originally dimension-less by definition (2).

Following Buchdahl [6, 7], we adopt two assumptions. One of them is a barotropic equation of state,

$$P = P(\Sigma) \, . \tag{4}$$

Hereafter, we regard the mass density Σ as an independent variable, and the others are functions of it,

$$R = R(\Sigma) \quad , \quad M = M(\Sigma) \quad , \quad P = P(\Sigma) \quad , \quad \Phi = \Phi(\Sigma) \,. \tag{5}$$

Another assumption is a non-increasing mass density in outward direction,

$$\frac{\mathrm{d}R(\Sigma)}{\mathrm{d}\Sigma} \leq 0 \,. \tag{6}$$

This implies the correspondence between variables R and Σ is one to one.

The surface of fluid ball is defined by vanishing pressure, where the hydrostatic equilibrium holds between fluid ball and outside vacuum region. Then, the mass density at surface Σ_* is determined by

$$P(\Sigma_*) = 0 \,, \tag{7}$$

and the total mass M_* and surface radius R_* of fluid ball are respectively given by

$$M_* = M(\Sigma_*) \quad , \quad R_* = R(\Sigma_*) \,. \tag{8}$$

At the centre of fluid ball, the mass density is unity $\Sigma_{\mathrm{c}} = 1$, and conditions, $R(1) = 0$ and $M(1) = 0$, should hold. Note that the mass density takes values in an interval,

$$\Sigma_* \leq \Sigma \leq 1 \,, \tag{9}$$

where the surface mass density satisfies $0 \leq \Sigma_* < 1$.

The outside region of fluid ball, $R > R_*$, is Schwarzschild geometry of mass M_*. The inside region, $R < R_*$, is determined by the Einstein equation and conservation law ${T^{\mu\nu}}_{;\nu} = 0$, which are reduced to Tolman-Oppenheimer-Volkoff (TOV) equations,

$$\frac{\mathrm{d}M(\Sigma)}{\mathrm{d}\Sigma} = 4\pi R(\Sigma)^2 \Sigma \frac{\mathrm{d}R(\Sigma)}{\mathrm{d}\Sigma} \tag{10a}$$

$$\frac{\mathrm{d}P(\Sigma)}{\mathrm{d}\Sigma} = A(M, R, P; \Sigma) \frac{\mathrm{d}R(\Sigma)}{\mathrm{d}\Sigma} \tag{10b}$$

$$\frac{\mathrm{d}\Phi(\Sigma)}{\mathrm{d}\Sigma} = -\frac{1}{\Sigma + P(\Sigma)} \frac{\mathrm{d}P(\Sigma)}{\mathrm{d}\Sigma} \,. \tag{10c}$$

where

$$A(M, R, P; \Sigma) := -\frac{[\,\Sigma + P(\Sigma)\,]\,[\,M(\Sigma) + 4\pi R(\Sigma)^3 P(\Sigma)\,]}{R(\Sigma)\,[\,R(\Sigma) - 2M(\Sigma)\,]} \,. \tag{11}$$

Given a concrete functional form of equation of state, two functions $R(\Sigma)$ and $M(\Sigma)$ are obtained by solving (10a) and (10b). Substituting those solutions into (10c), $\Phi(\Sigma)$ is obtained.

In addition to Buchdahl's assumptions (4) and (6), we assume subluminal condition of sound speed,

$$\frac{\mathrm{d}P(\Sigma)}{\mathrm{d}\Sigma} \leq 1 \,. \tag{12}$$

Given the above formulation, the remaining freedom is the functional form of $P(\Sigma)$ under the condition (12). Since the solution of TOV equations depend on the concrete form of $P(\Sigma)$, the value of total mass M_* and surface radius R_* of fluid ball vary with the concrete form of $P(\Sigma)$. In following sections, by the variation of functional form of $P(\Sigma)$ under the condition (12), a possible upper bound $\mathcal{B}$ of the ratio $M_*/R_*\,(= Gm_*/(c^2 r_*)\,)$ will be calculated,

$$\frac{M_*}{R_*} \le \mathcal{B}\,. \tag{13}$$

Using such variational method, our aim is to obtain the value of $\mathcal{B}$ lower than the Barraco-Hamity's bound $\mathcal{B}_{\rm BaHa} = 3/8$ which is lower than the famous Buchdahl's bound $\mathcal{B}_{\rm Buch} = 4/9$.

Here note that Barraco and Hamity [8] considered not only the Buchdahl's assumptions (4) and (6) but also the dominant energy condition which gives the following inequality for the perfect fluid ball,

$$P(\Sigma) \le \Sigma\,. \tag{14}$$

We expect that some physically reasonable (non-exotic) condition, which is more restrictive than the dominant energy condition, can decrease further the Barraco-Hamity's bound to a lower value. Concerning this expectation, let us point out that the subluminal-sound-speed condition (12) and definition of surface (7) predict the inequality (14) as well. The subluminal-sound-speed condition restricts not only the value of pressure such as inequality (14) but also the value of its differential such as inequality (12). This implies that the subluminal-sound-speed condition (12) is more restrictive than the dominant energy condition. Therefore, we expect that the subluminal-sound-speed condition is sufficient for us in search of an upper bound lower than Barraco-Hamity's bound.

2.2. Variational method: Strategy

The variational method which we are going to use is known as the optimal control theory. It has already been applied to an estimation of maximum mass of neutron star by Rhoades and Ruffini [12]. (See also [13, 14] for more details about application of the optimal control theory to neutron star mass.) We apply the optimal control theory to the search of upper bound $\mathcal{B}$ of inequality (13). However, we do not require readers to have knowledge of optimal control theory. All ideas of the variational analysis are explained below.

We introduce an auxiliary variable $U(\Sigma)$ by

$$\sin^2 U(\Sigma) := \frac{\mathrm{d}P(\Sigma)}{\mathrm{d}\Sigma}\,. \tag{15}$$

Then, the subluminal-sound-speed condition (12) is automatically satisfied, $\sin^2 U \le 1$. In order to make use of variational method, it is useful to express M_*/R_* by an integral form, ‡

$$\frac{M_*}{R_*} = \int_0^{R_*}\!\mathrm{d}R\,\frac{\mathrm{d}(M/R)}{\mathrm{d}R} = \int_{\Sigma_*}^{1}\!\mathrm{d}\Sigma\left(-\frac{\mathrm{d}(M/R)}{\mathrm{d}\Sigma}\right) =: \int_{\Sigma_*}^{1}\!\mathrm{d}\Sigma\, L\,, \tag{16a}$$

---

‡ The signature of (16a) is not $-\int \mathrm{d}R\,\mathrm{d}(M/R)/\mathrm{d}R$ but $+\int \mathrm{d}R\,\mathrm{d}(M/R)/\mathrm{d}R$, because of an inequality $\mathrm{d}(M/R)/\mathrm{d}R \ge 0$ which is found by $M/R \sim R^2$.

where the integrand L is arranged to the following form by using relation (15) and TOV equations ($10a$) and ($10b$),

$$L(M,R,P,U;\Sigma) = \frac{M - 4\pi R^3 \Sigma}{A(M,R,P;\Sigma) R^2} \sin^2 U \,. \tag{$16b$}$$

Our problem is to maximize the functional ($16a$) under three constraints; the relation (15) and TOV equations ($10a$) and ($10b$). In following discussion, ($10c$) is not considered, because Φ does not appear in the integrand L.

Because there are three constraints, we use the Lagrange's multiplier-method. Define a functional,

$$I := \int_{\Sigma_*}^{1} \mathrm{d}\Sigma [\, L + Y_{\mathrm{M}}(\Sigma)\, C_{\mathrm{M}} + Y_{\mathrm{R}}(\Sigma)\, C_{\mathrm{R}} + Y_{\mathrm{P}}(\Sigma)\, C_{\mathrm{P}} \,] \,, \tag{$17a$}$$

where functions $Y_{\mathrm{M}}(\Sigma)$, $Y_{\mathrm{R}}(\Sigma)$ and $Y_{\mathrm{P}}(\Sigma)$ are Lagrange multiplier, and C_{M}, C_{R} and C_{P} are defined according to the constraints ($10a$), ($10b$) and (15),

$$C_{\mathrm{M}}(M,R,P;\Sigma) = \frac{4\pi R(\Sigma)^2 \Sigma)}{A(M,R,P;\Sigma)} \sin^2 U(\Sigma) - \frac{\mathrm{d}M(\Sigma)}{\mathrm{d}\Sigma} \tag{$17b$}$$

$$C_{\mathrm{R}}(M,R,P;\Sigma) = \frac{1}{A(M,R,P;\Sigma)} \sin^2 U(\Sigma) - \frac{\mathrm{d}R(\Sigma)}{\mathrm{d}\Sigma} \tag{$17c$}$$

$$C_{\mathrm{P}}(M,R,P;\Sigma) = \sin^2 U(\Sigma) - \frac{\mathrm{d}P(\Sigma)}{\mathrm{d}\Sigma} \,. \tag{$17d$}$$

Extremal value of M_*/R_* is given by the condition $\delta I = 0$ under variations,

$$\begin{array}{rcl} M(\Sigma) & \to & M(\Sigma) + \delta M(\Sigma) \\ R(\Sigma) & \to & M(\Sigma) + \delta R(\Sigma) \\ P(\Sigma) & \to & M(\Sigma) + \delta P(\Sigma) \\ U(\Sigma) & \to & U(\Sigma) + \delta U(\Sigma) \,. \end{array} \tag{18}$$

Given the functional expression I of M_*/R_*, the strategy of our variational analysis consists of following steps:

step1 Divide the interval (9) of Σ into many infinitesimal intervals. Then, solve the equation $\delta I = 0$ in order to maximize the functional I at each infinitesimal interval.

step2 Integrate the maximized I of every infinitesimal interval of Σ. Then, we will obtain a formal expression of the upper bound $\mathcal{B} \geq M_*/R_*$ for the global interval (9).

step3 Calculate numerically the formal expression of $\mathcal{B}$ obtained in step2.

2.3. Variational method: Step1

We divide the interval (9) into many infinitesimal intervals. Look at one infinitesimal interval of Σ,

$$\Sigma_{\mathrm{d}} \leq \Sigma \leq \Sigma_{\mathrm{u}} \,, \tag{19}$$

where $\Sigma_* \leq \Sigma_{\mathrm{d}} < \Sigma_{\mathrm{u}} \leq 1$ and $\Sigma_{\mathrm{u}} - \Sigma_{\mathrm{d}} \ll 1$. Then, in the step1 of our variational analysis, we maximize M_*/R_* by solving $\delta I = 0$ under the variations (18) in the

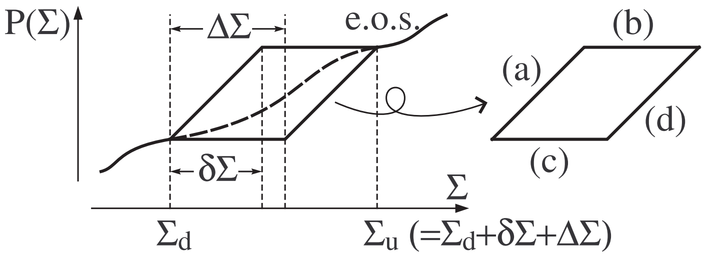

Figure 1. Extremization of M_*/R_* in an infinitesimal interval $\Sigma_{\rm d} \le \Sigma \le \Sigma_{\rm u}$. An original equation of state expressed by dashed curve is deformed to an extremal case of M_*/R_*, which forms an parallelogram.

interval (19). Note that, since we are considering a single interval (19) in the step1, we fix variables (M, R, P, U) in the remaining intervals, $\Sigma_* \le \Sigma < \Sigma_{\rm d}$ and $\Sigma_{\rm u} < \Sigma \le 1$. This indicates boundary conditions,

$$\delta X(\Sigma_{\rm d}) = 0 \quad , \quad \delta X(\Sigma_{\rm u}) = 0 \quad (X = M, R, P, U)\,. \tag{20}$$

The Euler-Lagrange equations of $\delta I = 0$ are followings: Variation of U gives

$$\Big[\frac{M - 4\pi R^3\Sigma}{AR^2} + Y_{\rm M}\frac{4\pi R^2\Sigma}{A} + Y_{\rm R}\frac{1}{A} + Y_{\rm P}\Big] \sin U\, \cos U = 0\,, \tag{21}$$

variations of $X(= M, R, P)$ give

$$-\frac{\partial Y_{\rm X}(\Sigma)}{\partial \Sigma} = \Big[\frac{\partial[\,(M - 4\pi R^3\Sigma)/(AR^2)\,]}{\partial X} + Y_{\rm M}\frac{\partial[\,4\pi R^2\Sigma/A\,]}{\partial X} + Y_{\rm R}\frac{\partial(1/A)}{\partial X}\Big] \sin^2 U\,, \tag{22}$$

and variations of $Y_{\rm X}$ give $C_X = 0$ which are constraints; TOV equations $(10a)$, $(10b)$, and relation (15). Equation (21) gives

$$U = 0\,, \frac{\pi}{2}\,, \tag{23}$$

or an algebraic equation given by vanishing the inside of square bracket of (21). However, the latter case (vanishing square bracket) is impossible under the boundary condition (20) as shown in Appendix A. Therefore, U should be constant given in (23), which denotes for extremal case of M_*/R_*,§

$$\frac{{\rm d}P(\Sigma)}{{\rm d}\Sigma} = 0\,, 1\,. \tag{24}$$

This gives a constant pressure or linear equation of state, $P(\Sigma) = \Sigma - \Sigma_*$. It is already revealed by Nilsson and Uggla [15] that, for the linear equation of state $(P = \Sigma - \Sigma_*)$, the total mass M_* and surface radius R_* are both finite for $\Sigma_* \ne 0$, but both infinite for $\Sigma_* = 0$. However, the behaviour of M_*/R_* has not been investigated so far.

---

§ In the case of Buchdahl's analysis [6], the maximum value $M_*/R_* = \mathcal{B}_{\rm Buch} = 4/9$ is realized for the fluid ball of constant mass density. The constant mass density implies that the sound speed is infinity. On the other hand, we are considering the subluminal-sound-speed condition. Therefore, the value 1 of sound speed for the extremal case of M_*/R_* in our analysis is consistent with Buchdahl's analysis.

Due to the extremal condition (24) and boundary condition (20), a parallelogram appears in Σ-P plane as show in figure 1. The equation of state given by edge (a)+(b) or (c)+(d) corresponds to a maximum or minimum value of M_*/R_* under the variations (18) in the infinitesimal interval (19). In order to judge which edge corresponds to maximum or minimum, we calculate their difference,

$$\Delta\Big(\frac{M_*}{R_*}\Big) := \int_{\rm (c)+(d)} {\rm d}\Sigma\, L - \int_{\rm (a)+(b)} {\rm d}\Sigma\, L\,, \tag{25a}$$

where the first term corresponds to an integral with equation of state given by the edge (c)+(d), and the second term is an integral with the edge (a)+(b). Here, note that TOV equations (10a) and (10b) result in that $M(\Sigma)$ and $R(\Sigma)$ are constant for $U = 0$ (${\rm d}P/{\rm d}\Sigma = 0$). Therefore, the edges (b) and (c) cause no contribution to M_*/R_*. Then, the difference $\Delta(M_*/R_*)$ is calculated to be

$$\begin{aligned}\Delta\Big(\frac{M_*}{R_*}\Big) &= \int_{\rm (d)} {\rm d}\Sigma\, L - \int_{\rm (a)} {\rm d}\Sigma\, L \\ &= L(M,R,P,U=1;\Sigma_{\rm d}+\Delta\Sigma)\,\delta\Sigma - L(M,R,P,U=1;\Sigma_{\rm d})\,\delta\Sigma \\ &= \frac{\partial L(M,R,P,U=1;\Sigma_{\rm d})}{\partial\Sigma_{\rm d}}\delta\Sigma\,\Delta\Sigma \\ &= \frac{R_{\rm d}-2M_{\rm d}}{R_{\rm d}(\Sigma_{\rm d}+P_{\rm d})^2}\delta\Sigma\,\Delta\Sigma > 0\,,\end{aligned} \tag{25b}$$

where $\delta\Sigma$ and $\Delta\Sigma$ correspond to two edges of parallelogram as shown in figure 1, and $M_{\rm d}$, $R_{\rm d}$ and $P_{\rm d}$ are mass, radius and pressure at $\Sigma_{\rm d}$. This inequality (25b) denotes that the equation of state with edge (c)+(d) (edge (a)+(b)) corresponds to the maximum (minimum) of M_*/R_* under variations in the infinitesimal interval (19) and boundary condition (20).

2.4. Variational method: Step2

Next, we proceed to an analysis in the global interval (9) of Σ. Consider a case that the values of pressure at centre, $P_{\rm c}$, and mass density at surface, Σ_*, are fixed. In this case, we can repeat the deformation of equation of state using an infinitesimally small parallelogram. Finally, the functional form of equation of state in interval (9) reaches one of following two options:

$$P(\Sigma) = \begin{cases} \Sigma - \Sigma_* & \text{in} \quad \Sigma_* \le \Sigma \le \Sigma_* + P_{\rm c} \\ P_{\rm c} & \text{in} \quad \Sigma_* + P_{\rm c} < \Sigma \le 1 \end{cases} \tag{26a}$$

$$P(\Sigma) = \begin{cases} 0 & \text{in} \quad \Sigma_* \le \Sigma < 1 - P_{\rm c} \\ \Sigma - (1-P_{\rm c}) & \text{in} \quad 1 - P_{\rm c} \le \Sigma \le 1 \end{cases}\,. \tag{26b}$$

These forms are shown in figure 2. No contribution to M_*/R_* causes from parts, $P =$ constant, as explained before calculating (25b). The inequality (25b) for infinitesimally small parallelogram indicates that the equation of state (26b) gives the maximum value of M_*/R_* for given $P_{\rm c}$ and Σ_*, whereas (26a) gives the minimum for given $P_{\rm c}$ and Σ_*.

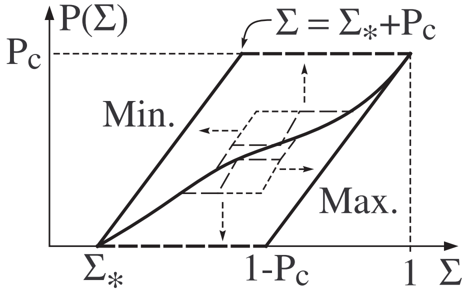

Figure 2. Maximization and minimization of M_*/R_* in the full interval $\Sigma_* \le \Sigma \le 1$ with fixing P_c and Σ_*. Horizontal dashed parts of e.o.s. do not contribute to M_*/R_*.

We should emphasize that the above discussion is applicable for only the case with fixed P_c and Σ_*. It has not been examined so far whether or not M_*/R_* for equation of state (26*b*) (or (26*a*)) is maximum (or minimum) even when the values of P_c and Σ_* vary. There is a possibility that a value of M_*/R_* for equations of state (26*a*) or (26*b*) for certain values of P_c and Σ_* is neither maximum nor minimum under variation of P_c and Σ_*.

In order to find a true maximum value of M_*/R_* under variation of P_c and Σ_*, we regard M_*/R_* for equation of state (26*b*) as a function of P_c,

$$f(P_\mathrm{c}) := \frac{M_*}{R_*} \text{ for equation of state } (26b)\,. \tag{27}$$

Here, note that the equation of state (26*b*) in the interval, $1 - P_\mathrm{c} \le \Sigma \le 1$, depends on only P_c. The maximum value of $f(P_\mathrm{c})$, which is denoted by $\mathcal{B}$, is the desired upper bound of mass-to-radius ratio, $M_*/R_* \le \mathcal{B}$. A numerical plot of $f(P_\mathrm{c})$ is going to be shown in next section 2.5.

In order to find a true minimum value of M_*/R_* under variation of P_c and Σ_*, we regard M_*/R_* for equation of state (26*a*) as a function of P_c and Σ_*. The minimum value of this function is the lower bound of M_*/R_*. Here, note that this lower bound can be read from $f(P_\mathrm{c})$ by following discussion: For the equation of state (26*a*) for given P_c and Σ_*, the quantity $\Sigma_* + P_\mathrm{c}$ can be regarded as a central mass density.‖ Then, following the normalization (3), we transform variables by $\widetilde{\Sigma} = \Sigma/(\Sigma_* + P_\mathrm{c})$, $\widetilde{P} = P/(\Sigma_* + P_\mathrm{c})$, $\widetilde{M} = \sqrt{\Sigma_* + P_\mathrm{c}}\, M$ and $\widetilde{R} = \sqrt{\Sigma_* + P_\mathrm{c}}\, R$. This transformation changes the form of equation of state (26*a*) in interval, $\Sigma_* \le \Sigma \le \Sigma_* + P_\mathrm{c}$, to the following form,

$$\widetilde{P}(\widetilde{\Sigma}) = \widetilde{\Sigma} - (1 - \widetilde{P}_\mathrm{c}) \quad \text{for} \quad 1 - \widetilde{P}_\mathrm{c} \le \widetilde{\Sigma} \le 1\,, \tag{28}$$

where $\widetilde{P}_\mathrm{c} := P_\mathrm{c}/(\Sigma_* + P_\mathrm{c})$. Furthermore, the form of TOV equations for transformed variables are the same with (10*a*) and (10*b*). Hence, the value of $\widetilde{M}_*/\widetilde{R}_*$ for equation of state (28) is equal to the value of M_*/R_* for equation of state (26*a*). On the other hand, the form of equation of state (28) is the same with equation of state (26*b*) in interval,

---

‖ We should also remember, $R(\Sigma) = $ constant for $P = $ constant due to TOV equations.

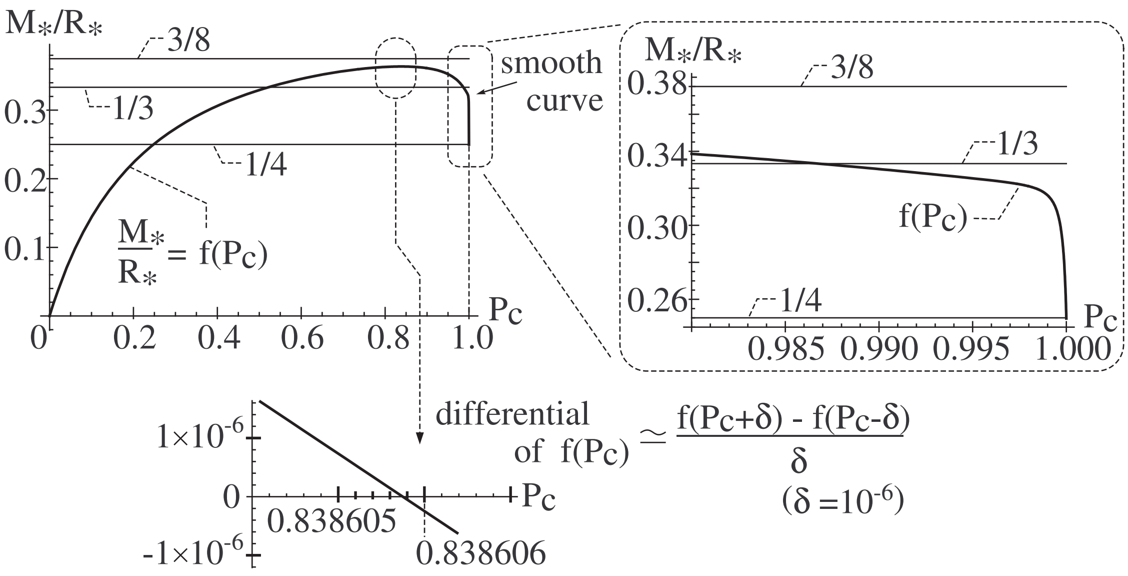

Figure 3. M_*/R_* as a function of P_c for linear equation of state (26*b*). Differential is plotted by an approximation, $\mathrm{d}f(P_\mathrm{c})/\mathrm{d}P_\mathrm{c} \simeq [\,f(P_\mathrm{c}+\delta)-f(P_\mathrm{c}-\delta)\,]/\delta$, where $\delta = 10^{-6}$. These plots are made with Mathematica ver.10.

$1 - P_\mathrm{c} \leq \Sigma \leq 1$. Therefore, the value of M_*/R_* for equation of state (26*a*) for given P_c and Σ_* is equal to that for equation of state (26*b*) with replacing P_c by $\widetilde{P}_\mathrm{c}$. This implies that the value of M_*/R_* for equation of state (26*a*) can be read from $f(P_\mathrm{c})$, and the minimum value of $f(P_\mathrm{c})$ is the lower bound of M_*/R_*.

2.5. Variational method: Step3

The function $f(P_\mathrm{c})$, defined in (27), can be calculated by following steps:

(i) Solve numerically TOV equations (10*a*) and (10*b*) with the equation of state (26*b*) for given value of P_c. A technical remark is summarized in Appendix B.

(ii) Calculate M_*/R_* from numerical solutions of step (i).

(iii) The function $f(P_\mathrm{c})$ is calculated by repeating steps (i) and (ii) for different values of P_c in the interval, $0 < P_\mathrm{c} \leq 1$.

Our numerical result is shown in figure 3. A smooth graph of $f(P_\mathrm{c})$ is obtained. From the plot of differential of $f(P_\mathrm{c})$ in figure 3, we find that the maximum of $f(P_\mathrm{c})$ is given at

$$P_\mathrm{c} = P_\mathrm{bound} \simeq 0.8386058\,. \tag{29}$$

Then, as discussed in previous section 2.4, the upper bound $\mathcal{B}_\mathrm{new} \geq M_*/R_*$ is given by the maximum value, $\mathcal{B}_\mathrm{new} \simeq f(P_\mathrm{bound})$, which is evaluated numerically to be $\mathcal{B}_\mathrm{new} \simeq 0.3636403$. This upper bound gives our conclusion (1). On the other hand, the lower bound read from figure 3 is zero given at $P_\mathrm{c} = 0$. No finite lower bound is found in our analysis.

3. Conclusion and discussions

By adding the subluminal-sound-speed condition (12) to Buchdahl's assumptions, we obtained figure 3 and the bound of mass-to-radius ratio of a barotropic fluid ball,

$$0 < \frac{M_*}{R_*} \le \mathcal{B}_{\rm new} \simeq 0.3636403\,. \tag{30}$$

This upper bound is lower than Barraco-Hamity's bound $\mathcal{B}_{\rm BaHa} = 3/8$. However, our upper bound is greater than $1/3\ (< \mathcal{B}_{\rm new})$, and there remains a possibility of an existence of super-compact object possessing unstable circular orbits of photons but no black hole horizon.

As read from figure 3, the upper bound $\mathcal{B}_{\rm new}$ corresponds to the central pressure, $P_{\rm c} = P_{\rm bound}$ of (29). This value of central pressure may be understood as a result of trade-off between pressure's two effects; a contribution to mass density (attractive force) and an effect pushing fluid outward (repulsive force).

From the above, the maximum value of M_*/R_* is $\mathcal{B}_{\rm new}$ of (30) which is obtained by solving the TOV equations with the central pressure $P_{\rm c} = P_{\rm bound}$ of (29) and linear equation of state (26*b*). Furthermore, by our numerical integration of TOV equations, the mass and radius of fluid ball in the case of maximum mass-to-radius ratio are

$$\begin{aligned} M_*(P_{\rm bound}) &= M_{\rm bound} &&\simeq 0.2014578 \\ R_*(P_{\rm bound}) &= R_{\rm bound} &&\simeq 0.5540028\,, \end{aligned} \tag{31}$$

which gives our bound $\mathcal{B}_{\rm new} = M_{\rm bound}/R_{\rm bound}$. From these values together with the normalization (3), we can estmate typical *un-normalized* values of physical quantitis for the case of maximum mass-to-radius ratio. With denoting the un-normalized mass in unit of solar mass, $m_{\rm bound} = \alpha M_\odot$, where α is a dimension-less factor, then the un-normalized central mass density $\sigma_{\rm bound}$, central pressure $p_{\rm bound}$ and radius $r_{\rm bound}$ are calculated as

$$\begin{aligned} \sigma_{\rm bound} &= \frac{c^6 M_{\rm bound}^2}{G^3 m_{\rm bound}^2} &&\simeq \frac{2.5}{\alpha^2} \times 10^{16}\ \ {\rm g/cm^3} \\ p_{\rm bound} &= \sigma_{\rm bound} c^2 P_{\rm bound} &&\simeq \frac{1.3}{\alpha^2} \times 10^{39}\ \ {\rm GeV/cm^3} \\ r_{\rm bound} &= \frac{G m_{\rm bound}}{c^2 \mathcal{B}_{\rm new}} &&\simeq 4.1\,\alpha\ \ {\rm km}\,. \end{aligned} \tag{32}$$

Note that, the case of maximum mass-to-radius ratio corresponds to the linear equation of state (26*b*) giving the luminal (equal-to-light) sound speed inside the fluid ball. If the equation of state, $P(\Sigma)$, will be restricted to some functional form other than the linear form, then the upper bound $\mathcal{B}$ of M_*/R_* will take a value different from $\mathcal{B}_{\rm new}$ of (30). We will report the case of polytropic equation of state in the other paper.¶

¶ We will show in the other paper that, when the equation of state is restricted to be the polytropic one ($P(\Sigma) \propto \Sigma^{1+1/n}$) under the subluminal-sound-speed condition, the maximum value of M_*/R_* becomes a value lower than $\mathcal{B}_{\rm new}$ of (30), $M_*/R_* \le 0.281$. In deriving this result of polytrope, we will not use the variational method, but use the other numerical search method.

Finally we make a mathematical comment on a limiting behaviour found from figure 3,

$$\lim_{P_\mathrm{c}\to 1} f(P_\mathrm{c}) = \frac{1}{4}\,. \tag{33}$$

At the limit $P_\mathrm{c} \to 1$, the equation of state (26*b*) asymptotes to a simple form $P(\Sigma) = \Sigma$ $(0 \le \Sigma \le 1)$. Further, functional forms of $M(\Sigma)$ and $R(\Sigma)$ converge to an exact solution of TOV equations with equation of state $P(\Sigma) = \Sigma$;

$$M(\Sigma) = \frac{1}{4} R(\Sigma) = \frac{1}{16\sqrt{\pi\Sigma}}\,. \tag{34}$$

This results in a finite limit (33). However, the total mass and surface radius of fluid ball diverge $M_* \to \infty$ and $R_* \to \infty$ as $P_\mathrm{c} \to 1$, because the surface mass density is zero, $\Sigma_* \to 0$ as $P_\mathrm{c} \to 1$. This result is consistent with Nilsson-Uggla's numerical result [15] that, for the linear equation of state, $P = \Sigma - \Sigma_*$ $(\Sigma_* = 1 - P_\mathrm{c})$, the mass M_* and radius R_* are both finite for $\Sigma_* \neq 0$ but diverge as $\Sigma_* \to 0$.

Acknowledgments

We would like to express our gratitude to Tomohiro Harada, since a communication with him lets us to notice the use of variational method. H.S. was supported by Japan Society for the Promotion of Science (JSPS), Grant-in-Aid for Scientific Research (KAKENHI, Exploratory Research, 26610050).

Appendix A. Impossibility of vanishing square bracket of (21)

In this appendix, we show that, as a solution of (21), the vanishing square bracket of (21) is impossible under the boundary condition (20).

Assume that a solution of (21) is given by vanishing the square bracket, we find

$$Y_\mathrm{P} = -\frac{1}{A(M,R,P;\Sigma)}\left[Y_\mathrm{R} + \frac{M}{R^2} + 4\pi R^2\,\Sigma\left(Y_\mathrm{M} - \frac{1}{R}\right)\right]. \tag{A.1}$$

On the other hand, we obtain from (22),

$$\frac{\mathrm{d}Y_\mathrm{M}}{\mathrm{d}\Sigma} = -\frac{R + 8\pi R^3 P}{(R-2M)(M+4\pi R^3 P)} Y_\mathrm{P}\,\sin^2 U - \frac{\sin^2 U}{A(M,R,P;\Sigma)R^2} \tag{A.2}$$

$$\begin{aligned}\frac{\mathrm{d}Y_\mathrm{R}}{\mathrm{d}\Sigma} &= \left(\frac{1}{R} + \frac{1}{(R-2M)} - \frac{12\pi R^2 P}{M + 4\pi R^3 P}\right) Y_\mathrm{P}\sin^2 U \\ &\quad + \left[\frac{2M}{R^3} + 4\pi\Sigma\Big(1 - 2RY_\mathrm{M}\Big)\right]\frac{\sin^2 U}{A(M,R,P;\Sigma)}\end{aligned} \tag{A.3}$$

$$\frac{\mathrm{d}Y_\mathrm{P}}{\mathrm{d}\Sigma} = -\frac{M\Sigma + 4\pi R^3(P\Sigma + \Sigma + P)}{(\Sigma+P)(M+4\pi R^3 P)} Y_\mathrm{P}\sin^2 U\,. \tag{A.4}$$

Equation (A.4) with boundary condition (20) results in $Y_\mathrm{P} = 0$. Then (A.1) gives

$$Y_\mathrm{R} + \frac{M}{R^2} + 4\pi R^2\,\Sigma\left(Y_\mathrm{M} - \frac{1}{R}\right) = 0\,. \tag{A.5}$$

Differentiate this equation by Σ and substitute (A.2), (A.3) and TOV equations (10*a*) and (10*b*), we obtain

$$Y_{\rm M}(\Sigma) = \frac{1}{R(\Sigma)} \quad , \quad Y_{\rm R}(\Sigma) = -\frac{M(\Sigma)}{R(\Sigma)^2} \, , \tag{A.6}$$

where $Y_{\rm R}$ is obtained by substituting $Y_{\rm M}$ in (A.5). These solutions cannot satisfy the boundary condition (20). Hence, the solution of (21) is given by (23).

Appendix B. On numerical treatment of TOV equations

Right-hand sides of TOV equations (10*a*) and (10*b*) are indeterminate form at centre because of the conditions, $M \to 0$ and $R \to 0$ as $\Sigma \to 1$. Therefore, in solving TOV equations numerically in step (i) of section 2.5, we have made use of perturbative solutions near the centre.

In order to consider a perturbation near centre, we regard the radius R as an independent variable, and the mass density as a function of radius, $\Sigma(R)$. TOV equations (10*a*) and (10*b*) are rearranged to the following forms,

$$\frac{\mathrm{d}M(R)}{\mathrm{d}R} = 4\pi R^2 \Sigma(R) \quad , \quad \frac{\mathrm{d}P(R)}{\mathrm{d}R} = -\frac{[\,\Sigma(R) + P(R)\,]\,[\,M(R) + 4\pi R^3 P(R)\,]}{R\,[\,R - 2M(R)\,]} \, . \tag{B.1}$$

For a sufficiently small radius $R \ll 1$, we introduce perturbations,

$$\begin{aligned} M(R) &= M_{(1)} R + M_{(2)} R^2 + M_{(3)} R^3 + \cdots \\ P(R) &= P_{\rm c} + P_{(1)} R + P_{(2)} R^2 + P_{(3)} R^3 + \cdots \\ \Sigma(R) &= 1 + \Sigma_{(1)} R + \Sigma_{(2)} R^2 + \Sigma_{(3)} R^3 + \cdots \, , \end{aligned} \tag{B.2}$$

where conditions $M(R=0) = 0$, $\Sigma(R=0) = 1$ and $P(R=0) = P_{\rm c}$ are included. Substituting (B.2) into (B.1), we obtain $M_{(1)} = 0$, $M_2 = 0$, $P_{(1)} = 0$ and remaining parts,

$$\begin{aligned} M(R) &= \frac{4}{3}\pi R^3 + \pi \Sigma_{(1)} R^4 + \cdots \\ P(R) &= P_{\rm c} - \frac{2}{3}\pi (1 + 3P_{\rm c})\,(1 + P_{\rm c}) R^2 - \frac{\pi}{9}(7 + 15P_{\rm c}) \Sigma_{(1)} R^3 + \cdots \\ \Sigma(R) &= 1 + \Sigma_{(1)} R + \Sigma_{(2)} R^2 + \Sigma_{(3)} R^3 + \cdots \, , \end{aligned} \tag{B.3}$$

where the central pressure $P_{\rm c}$ and coefficients $\Sigma_{(n)}$ $(n = 1, 2, 3, \cdots)$ are determined by the concrete form of equation of state.

Comparing $P(R)$ in (B.3) with equations of state (26*b*), we obtain $\Sigma_{(1)} = 0$ and $\Sigma_{(2)} = P_{(2)}$. Hence, denoting a small radius by $R_\delta \ll 1$, the mass density Σ_δ and mass M_δ at $R = R_\delta$ are approximately given by

$$\Sigma_\delta = 1 - \frac{2}{3}\pi (1 + 3P_{\rm c})\,(1 + P_{\rm c}) R_\delta^2 \quad , \quad M_\delta = \frac{4}{3}\pi R_\delta^3 \, . \tag{B.4}$$

If the mass density near centre Σ_δ is given, the others are determined by

$$R_\delta = \sqrt{\frac{3(1 - \Sigma_\delta)}{2\pi (1 + 3P_{\rm c})(1 + P_{\rm c})}} \quad , \quad M_\delta = \frac{4}{3}\pi \left(\frac{3(1 - \Sigma_\delta)}{2\pi (1 + 3P_{\rm c})(1 + P_{\rm c})} \right)^{3/2} \, . \tag{B.5}$$

In step (i) of section 2.5, we have solved TOV equations $(10a)$ and $(10b)$ in an interval, $\Sigma_* \leq \Sigma \leq \Sigma_\delta$, with initial condition (B.5). Also, the convergence of numerical solutions has been checked by varying Σ_δ. Our results in figure 3 are made using $\Sigma_\delta = 1 - 10^{-6}$.

References

[1] Takahashi R 2004 Shapes and positions of black hole shadows in accretion disks and spin parameters of black holes *Astrophys. J.* **611** 996

[2] Kanai K and Nambu Y 2013 Viewing black holes by waves *Class. Quantum Grav.* **30** 175002

[3] Miyoshi M, Ishitsuka J K, Kameno S, Shen Z and Horiuchi S 2004 Direct imaging of the massive black hole SgrA* *Prog. Theor. Phys. Suppl.* **155** 186

[4] Doeleman S S *et al* 2008 Event-horizon-scale structure in the supermassive black hole candidate at the galactic centre *Nature* **455** 78

[5] Sakai N, Saida H and Tamaki T 2014 Gravastar shadows *Phys. Rev.* D **90** 104013

[6] Buchdahl H A 1959 General relativistic fluid spheres *Phys. Rev.* **116** 1027

[7] Wald R M 1984 *General Relativity* (Chicago: The Univ. of Chicago Press) §6.2

[8] Barraco D and Hamity V H 2002 Maximum mass of a spherically symmetric isotropic star *Phys. Rev.* D **65** 124028

[9] Böhmer C G 2005 Static perfect fluid balls with given equation of states and cosmological constant *Ukr. J. Phys.* **50** 1219

[10] Hod S 2007 Bounds on the mass-to-radius ratio for non-compact field configurations *Class. Quantum Grav.* **24** 6019

[11] Andréasson H 2008 Sharp bounds on $2m/r$ of general spherically symmetric static object *J. Diff. Eq.* **245** 2243

[12] Rhoades C E Jr. and Ruffini R 1974 Maximum mass of a neutron star *Phys. Rev. Lett.* **32** 324

[13] Rhoades C E Jr. and Ruffini R 1973 On the maximum mass of a neutron star, *Appendix 1.3* of the book *Les Houches Summer School, Black Holes* edited by DeWitt C and DeWitt B S (New York: Gordon and Breach Science Publishers)

[14] Pietronero L and Ruffini R 1978 On the maximum mass of a neutron star, in the book *Physics and Astrophysics of Neutron stars and Black Holes* edited by Giacconi R and Ruffini R (Amsterdam: North Holland Publishing)

[15] Nilsson U S and Uggla C 2001 General relativistic stars: linear equations of state *Annals Phys.* **286** 278